Electronic Supplementary Material (ESI) for Physical Chemistry Chemical Physics.

# Electronic Supplementary Information

# The Mechanism of $Mg^{2+}$ Conduction in Ammine Magnesium Borohydride Promoted by a Neutral Molecule

Yigang Yan,[ab#] Wilke Dononelli,[c#] Mathias Jørgensen,[a] Jakob B. Grinderslev,[a] Young-Su Lee,[d] Young Whan Cho,[d] Radovan Černý,[e] Bjørk Hammer,[c] Torben R. Jensen[a*]

*[a]Interdisciplinary Nanoscience Center (iNANO) and Department of Chemistry, Aarhus University, Langelandsgade 140, 8000 Aarhus C, Denmark. E-mail: trj@chem.au.dk.*
*[b]Institute of New Energy and Low-Carbon Technology, Sichuan University, Chengdu 610207, China.*
*[c]Department of Physics and Astronomy and Interdisciplinary Nanoscience Center (iNANO), Aarhus University, 8000 Aarhus, Denmark.*
*[d]Center for Energy Materials Research, Korea Institute of Science and Technology, Seoul 02792, Republic of Korea.*
*[e]Department of Quantum Matter Physics Laboratory of Crystallography University of Geneva Quai Ernest-Ansermet 24 1211 Geneva, Switzerland.*

* Corresponding author: Torben R. Jensen (e-mail: trj@chem.au.dk)
[#] These authors contributed equally to this work.

## Phase identification

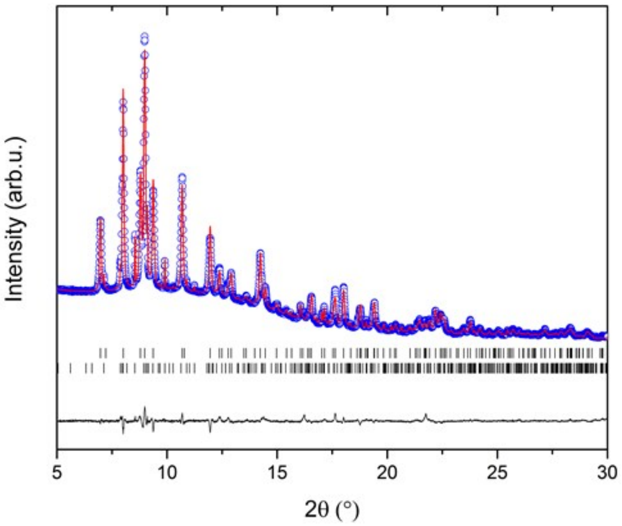

**Figure S1.** Rietveld refinement of PXD data measured at room temperature for $Mg(BH_4)_2{\cdot}NH_3$, showing experimental (blue circles) and calculated (red line) PXD patterns, and a difference plot below (black line). Top tick ($Mg(BH_4)_2{\cdot}NH_3$, 89.8 %), bottom tick ($\alpha$-$Mg(BH_4)_2$, ICSD_162974, 10.2 %). Final discrepancy factors: $R_p = 1.15$ %, $R_{wp} = 1.73$ % (not corrected for background), $R_p = 8.92$ %, $R_{wp} = 8.94$ % (conventional Rietveld *R*-factors), $R_{Bragg}(Mg(BH_4)_2{\cdot}NH_3) = 3.58$ %, $R_{Bragg}(\alpha\text{-}Mg(BH_4)_2) = 6.85$ % and global $\chi^2 = 5.45$ ($\lambda = 0.708481$ Å).

**Table S1.** Structure data of $Mg(BH_4)_2{\cdot}NH_3$ extracted from Rietveld refinement in Fig. S1. Space group: *Pnma*, lattice parameters: $a = 11.2938(1)$, $b = 7.6224(1)$, $c = 6.8182(1)$ Å.

| Atom | x / a | y / b | z / c | Wyckoff site | Occupancy |
|---|---|---|---|---|---|
| B1 | 0.50000 | 0.50000 | 0.50000 | 4a | 1 |
| H11 | 0.56403 | 0.41279 | 0.39145 | 8d | 0.5 |
| H12 | 0.53049 | 0.65397 | 0.49965 | 8d | 0.5 |
| H13 | 0.50477 | 0.44475 | 0.66684 | 8d | 0.5 |
| H14 | 0.40029 | 0.48929 | 0.44337 | 8d | 0.5 |
| B2 | 0.1908(3) | 0.75000 | 0.5201(4) | 4c | 1 |
| H21 | 0.0907(3) | 0.75000 | 0.5792(4) | 4c | 1 |
| H22 | 0.2594(3) | 0.75000 | 0.6609(4) | 4c | 1 |
| H23 | 0.2078(3) | 0.87959 | 0.4201(4) | 8d | 1 |
| N | 0.6283(3) | 0.25000 | 0.8916(4) | 4c | 1 |
| H31 | 0.5937(3) | 0.36051 | 0.9422(4) | 8d | 1 |
| H32 | 0.7089(3) | 0.25000 | 0.9486(4) | 4c | 1 |
| Mg | 0.6210(2) | 0.25000 | 0.5939(2) | 4c | 1 |

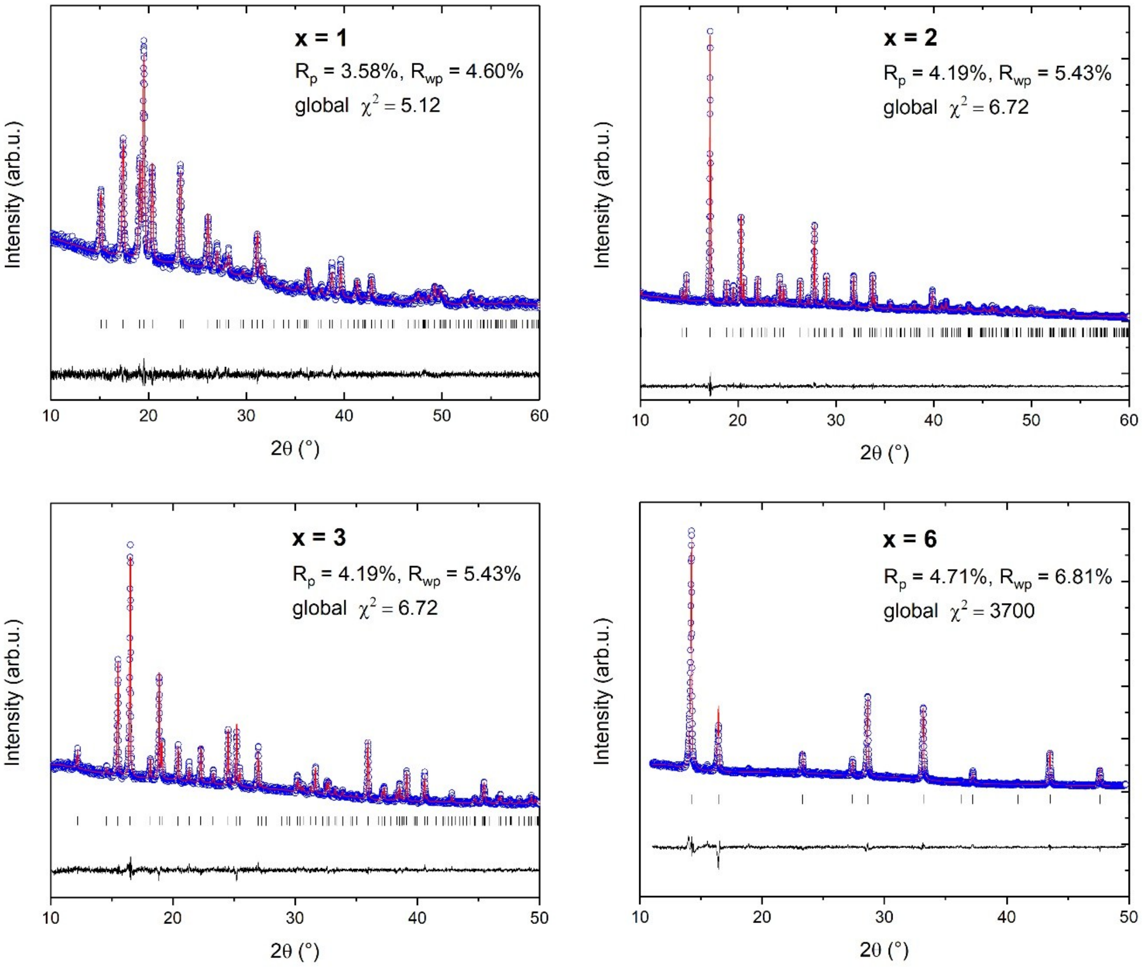

**Figure S2.** Rietveld refinement of PXD data measured at room temperature for $Mg(BH_4)_2 \cdot xNH_3$ ($x$ = 1, 2, 3, 6), showing experimental (blue circles) and calculated (red line) PXD patterns, and a difference plot below (black line) (λ = 1.54056 Å). Final discrepancy factors, $R_p$ and $R_{wp}$ (not corrected for background), and global $\chi^2$ are shown. $Mg(BH_4)_2 \cdot NH_3$: space group *Pnma*, unit cell parameters *a* = 11.2938(1), *b* = 7.6224(1), *c* = 6.8182(1) Å. $Mg(BH_4)_2 \cdot 2NH_3$: space group *Pcab*, unit cell parameters *a* = 17.4872(4), *b* = 9.4132(2), *c* = 8.7304(2) Å. $Mg(BH_4)_2 \cdot 3NH_3$: space group *Pnma*, unit cell parameters *a* = 11.4186(2), *b* = 8.0673(1), *c* = 9.3868(1) Å. $Mg(BH_4)_2 \cdot 6NH_3$: space group *Fm*-3*m*, unit cell parameters *a* = *b* = *c* = 10.7879(1) Å.

## The nature of the di-hydrogen bond

Hydrogen bonds are conventionally formed between a proton donator (often N–H, O–H or F–H) and an acceptor group which is usually a lone pair of either nitrogen or oxygen. In addition the partially negatively charged H atoms in metal hydrides and boron hydrides can act as acceptor groups to form di-hydrogen bonds.[1,2] In all systems presented in this study, borohydride and ammonia are present in the crystal structures. Therefore, if di-hydrogen bonds are present they might be responsible for stabilizing the structures or influencing the ionic conductivity of the materials. In order to investigate the nature of the di-hydrogen bond with calculations, we first set up a model system containing one $NH_3$ molecule and a $BH_4^-$ complex. The cell parameters were fixed to $x = y = 10$ Å and $z = 25$ Å. The H–H distance of one H atom of $NH_3$ and another H atom of $BH_4^-$ was varied between 1 Å and 10 Å.

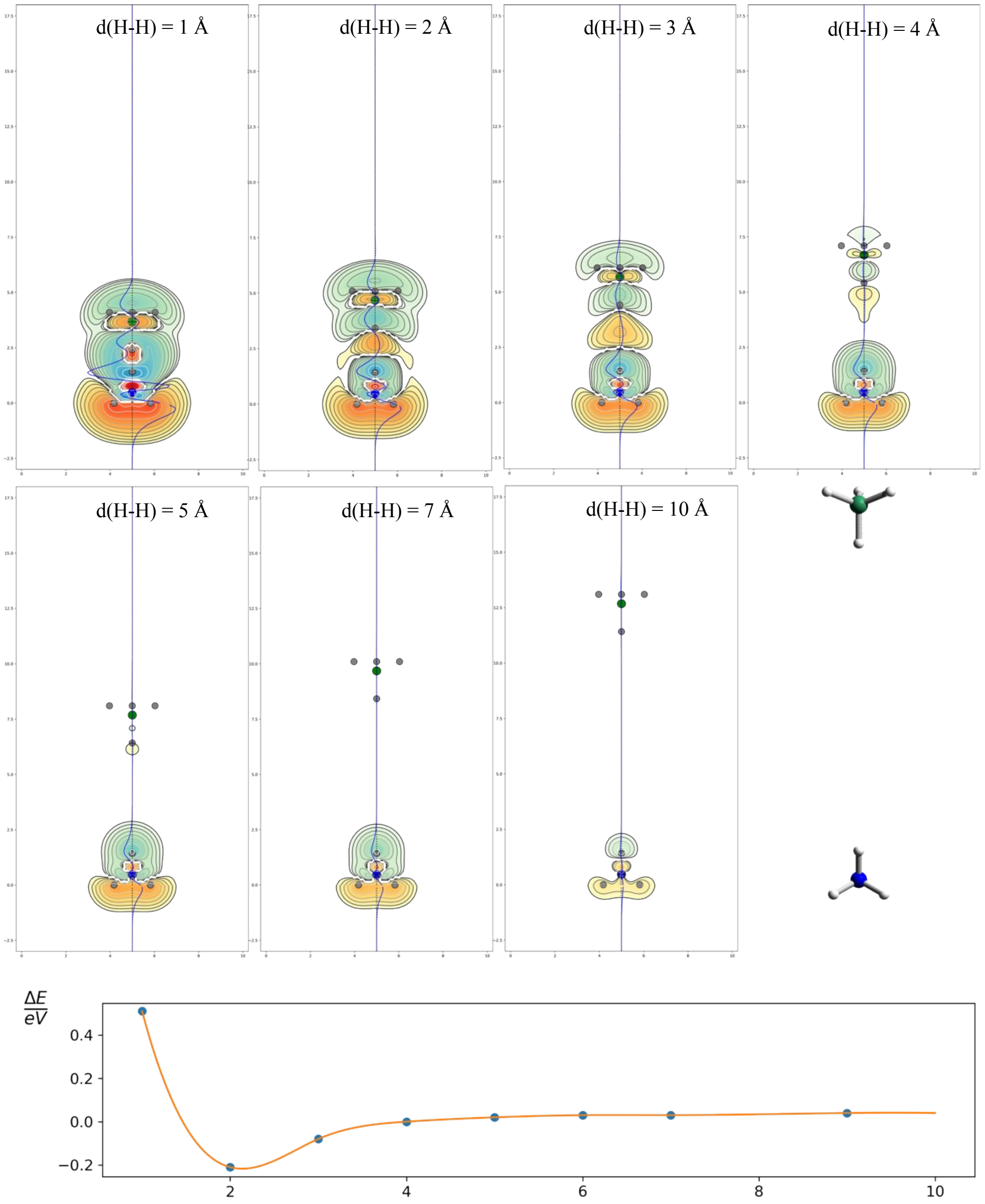

**Figure S3.** Electron density differences of a model system containing $NH_3$ and $BH_4^-$ at different H–H-distances ranging from 1 Å to 10 Å. **Top**: green spots denote boron, blue spots nitrogen and grey spots hydrogen atoms. Increase of electron density is shown in yellow to red contour lines, while decrease is shown in green to blue contours; The blue curve corresponds to the integrated electron density on the straight dotted line along the bonding H–H-axis. Values to the right of the vertical dotted line correspond to increase of electron density, values to the left to decrease of electron density; **Bottom**: interaction energies (in eV) for $NH_3$ and $BH_4^-$ for H–H distances in a range between 1 Å and 10 Å. Blue spots are calculated values, orange are interpolated values.

In Fig. S3 top) the integrated electron density difference of interacting and non-interacting $NH_3$ and $BH_4^-$ is shown. These electron density differences reveal the nature of the bond between two atoms. In case of hydrogen bonding also polarization needs to be considered. Bader analysis gave a partial positive charge (~0.5 *e*) for H atoms of $NH_3$ and partial negative charge (~ − 0.5*e*) for H atoms of $BH_4^-$. These results were found for the model system, separately calculated species and the real system.

Even at far distance of *d*(H–H) = 10 Å (see Fig. S3 top) $NH_3$ is polarised resulting in a partial electron transfer from the hydrogen atom pointing towards $BH_4^-$ to the other two H atoms of $NH_3$. When moving towards each other polarization within $NH_3$ gradually gets stronger. Starting from *d*(H–H) = 4 Å, a polarization of $BH_4^-$ is found in addition. Electron density is taken from the B–H bond in $BH_4^-$ and transferred towards the partially positively charged H atom of $NH_3$. Going down to a minimum energy H–H distance of 2 Å ($\Delta E$ = –0.21 eV) polarization is complete and charge is partially transferred from boron hydride to ammonia. Going further down to a H–H-distance of 1 Å, interestingly, the charge which was transferred between the H–H dihydrogen bond is now transferred to the H atom of $BH_4^-$. Note however, here an interaction energy of 0.51 eV, thus a repulsive character, was found.

The findings from this model system can now be used in order to analyze the role of the dihydrogen bond in $Mg(BH_4)_2{\cdot}NH_3$. Here the H–H distances between a H atom of $BH_4^-$ and a H atom of $NH_3$ in the equilibrium geometry is smaller with 1.84 - 2.1 Å compared to the model system with ~2 - 2.6 Å. This can be explained by *i*) the bonding of ammonia to more than one boronhydride and *ii*) the interaction with the positively charged $Mg^{2+}$ ion, which attracts some of the electron density.

As seen in Fig. S4, a complex system of di-hydrogen bonds stabilises ammonia molecules at their lattice positions (see dotted lines in Fig. S4 right). During the migration of an interstitial magnesium ion, the dihydrogen bond is responsible for keeping ammonia close to its lattice position and preventing migration of ammonia through the material.

Small barriers of 0.1-0.2 eV in the migration pathway shown in Fig. 3 in the main text can be explained by rotation of $BH_4^-$ groups along with a breaking and formation of a hydrogen bond. When $Mg^{2+}$ migrates, and detaches from $NH_3$, the ammonia is pulled back to its lattice position.

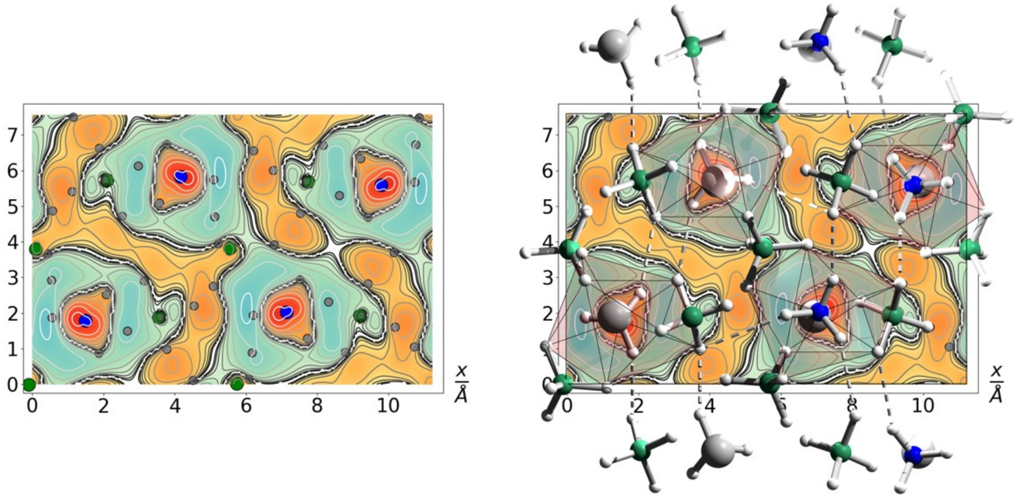

**Figure S4.** Charge density difference of $Mg(BH_4)_2{\cdot}NH_3$ including four formula units in the calculations, i.e. $Mg_4(BH_4)_8(NH_3)_4$. Electron density differences were calculated from the densities of $[(BH_4)_8(NH_3)_4]^{8-}$, $[(BH_4)_8]^{8-}$ and $[(NH_3)_4]$ with atoms positions of the relaxed $Mg_4(BH_4)_8(NH_3)_4$ structure.

## Thermal properties of $Mg(BH_4)_2 \cdot xNH_3$

Compounds $x = 1$ and $x = 2$, show the melting point at 90 and 110 ℃, respectively (Fig. S5). The onset decomposition temperature of compound $x = 3$ was observed to be ~ 120 ℃ [3] and the onset decomposition temperature of compound $x = 6$ was measured to be around 70 ℃.[4]

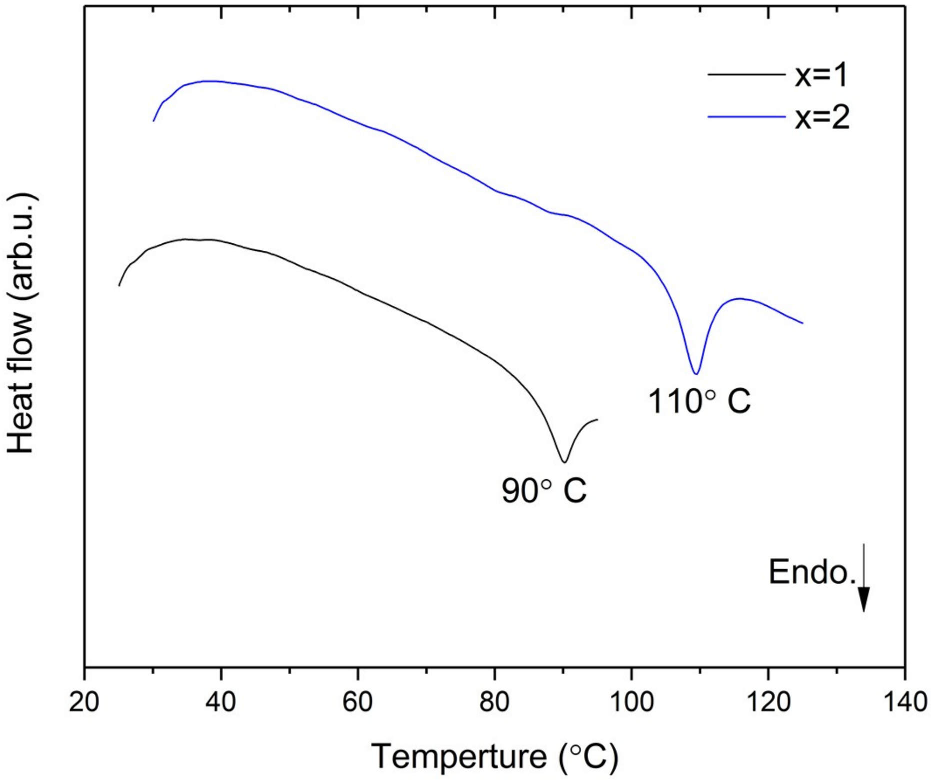

**Figure S5.** Differential scanning calorimetry profiles of samples $Mg(BH_4)_2 \cdot xNH_3$ ($x = 1, 2$) measured in an argon flow (50 mL/min) with a heating rate of $\Delta T/\Delta t = 5$ °C/min.

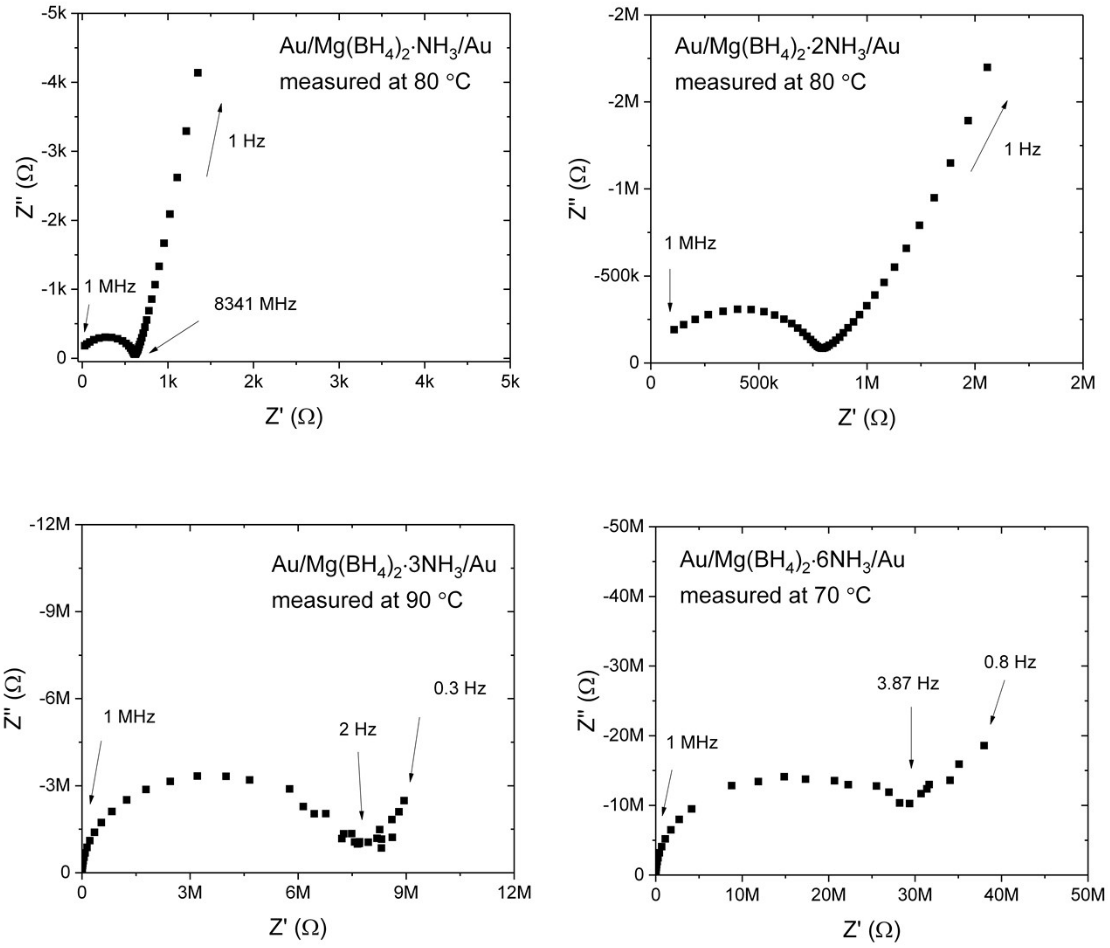

**Figure S6.** Nyquist plots of for $Mg(BH_4)_2 \cdot x NH_3$ ($x = 1, 2, 3, 6$) at selected temperatures, which consist of a semi circle and a spike.

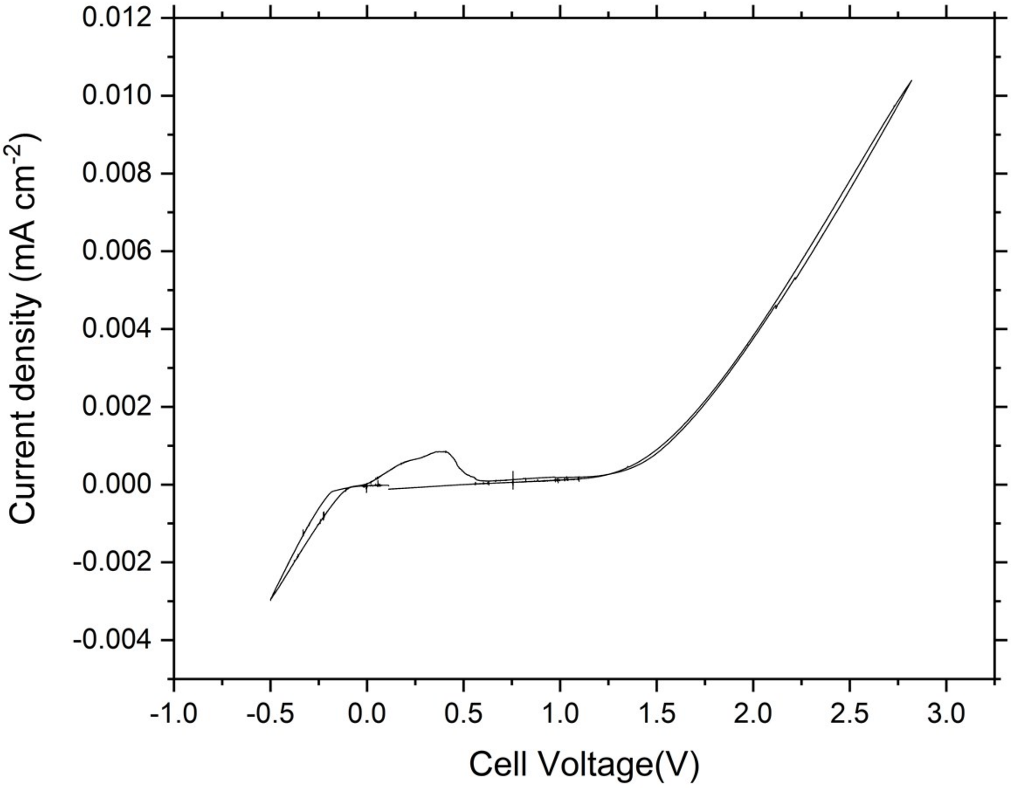

**Figure S7**. Cyclic voltammogram of an Au| $Mg(BH_4)_2{\cdot}NH_3$|Mg cell at 80 °C. The irreversible oxidation was observed to start around 1.3 V.

## Detailed analysis of the magnesium migration pathway

Here we present the entire $Mg^{2+}$ migration pathway through the unit cell. In Fig. S8, the energy profile and structures of all meta-stable intermediate structures with interstitial magnesium are shown (denoted **a**, **b**, **c** *etc*.). Structures of selected transition states are also included (denoted **a'**, **b'**, **c'** *etc*.). In the initial (**a**) and final (**n**) state, the magnesium interstitial is 8-fold (8f) coordinated (see coordination numbers (CN) in Table S2). The lattice magnesium ions are displaced up to 2.68 Å from their original position, as the interstitial Mg approach that position. After the interstitial Mg moves far enough away, the lattice Mg is able to move back to its original position (**e**→**h**).

The migration mechanism of interstitial $Mg^{2+}$ includes three distinct types of steps: *i*) exchange of coordinated ammonia molecules, *ii*) displacement of framework magnesium ions and *iii*) exchange of coordinated $BH_4^-$. All steps of interstitial Mg migration also involve minor reorientation of $BH_4^-$, which occur by reformation of di-hydrogen bonds.

The structure of $Mg(BH_4)_2 \cdot NH_3$ reveals a high degree of flexibility owing to the relatively free exchange of ammonia among Mg ions and the varying $BH_4^-$ coordination ($\eta^1$, $\eta^2$, or $\eta^3$). This is evident from lattice Mg displacements of up to 2.68 Å and the different interstitial Mg coordination environments observed throughout the migration pathway (meta-stable structures **a** to **n**. The coordination of interstitial Mg includes four distinct environments, *i*) a tetragonal coordination to three $BH_4^-$ and one $NH_3$ (**a, f, i, n**), *ii*) a trigonal bipyramidal coordination to three $BH_4^-$ and two $NH_3$ (**d**), *iii*) a trigonal bipyramidal coordination to four $BH_4^-$ and one $NH_3$ (**g**, **h**), and *iv*) a trigonal planar coordination to three $BH_4^-$ (**k**, **l**), see Fig. S8). Furthermore, the lattice Mg is generally stabilised in a tetrahedral coordination to four $BH_4^-$, similar to that found in the structure of $Mg(BH_4)_2$, during transfer of ammonia to the interstitial magnesium (*e.g.* **b**). Di-hydrogen bonds are suggested to play a crucial role in stabilising these intermediate states, despite their relatively weak bond strength, due to their contribution to structural flexibility. The structural flexibility allow reorientation of ammonia molecules and borohydride complexes.

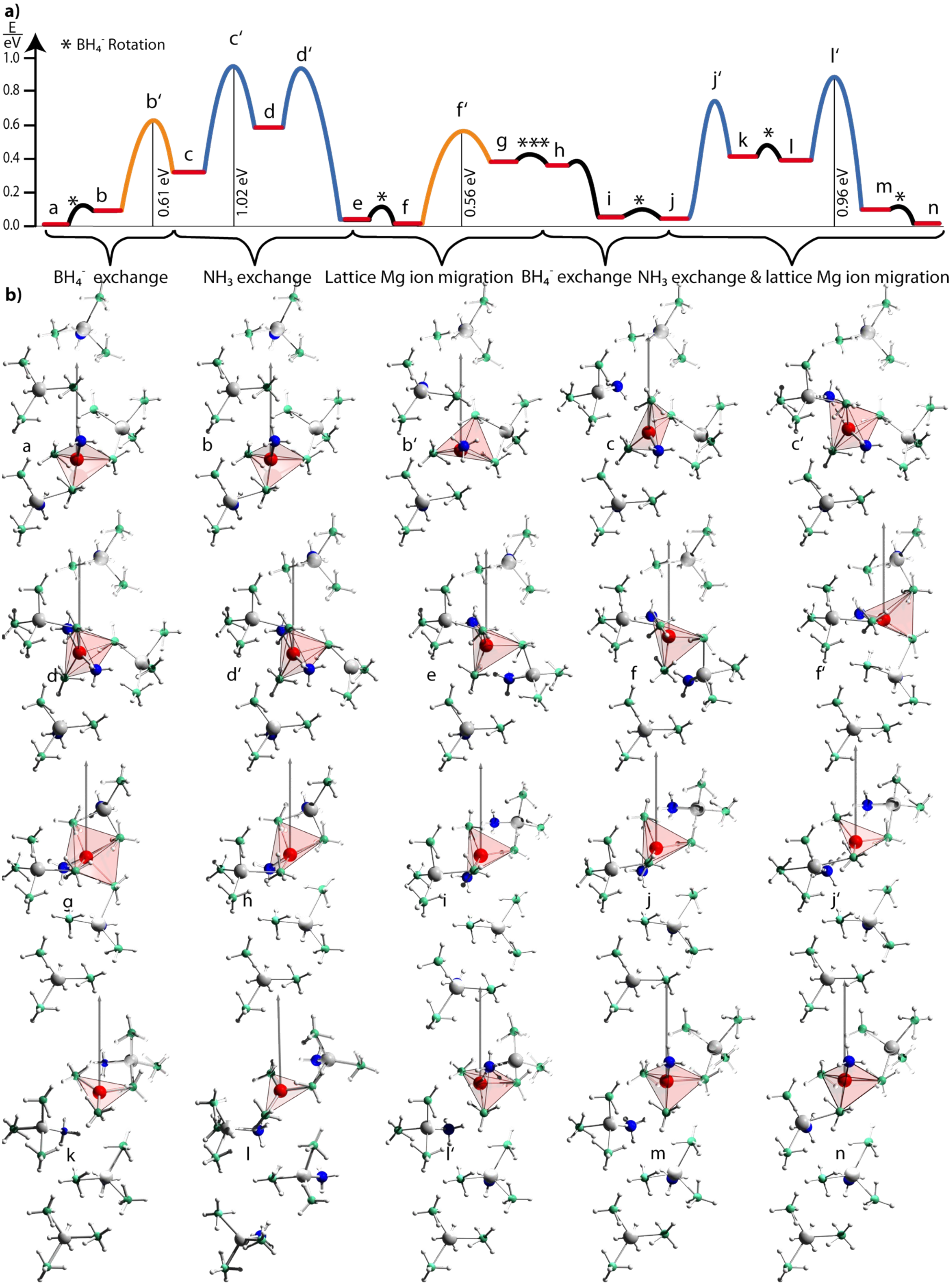

**Figure S8.** Migration pathway of $Mg^{2+}$ in $Mg(BH_4)_2{\cdot}NH_3$. **a)** Energy profile for the migration pathway calculated at PBE level of theory. * denotes rotation of $BH_4^-$ **b)** Structural 'snapshots' of the most important local minima and transition states of the 70 images used for NEB calculations in total. Only the part of the structure involved in the migration of $Mg^{2+}$ in the unit cell is shown.

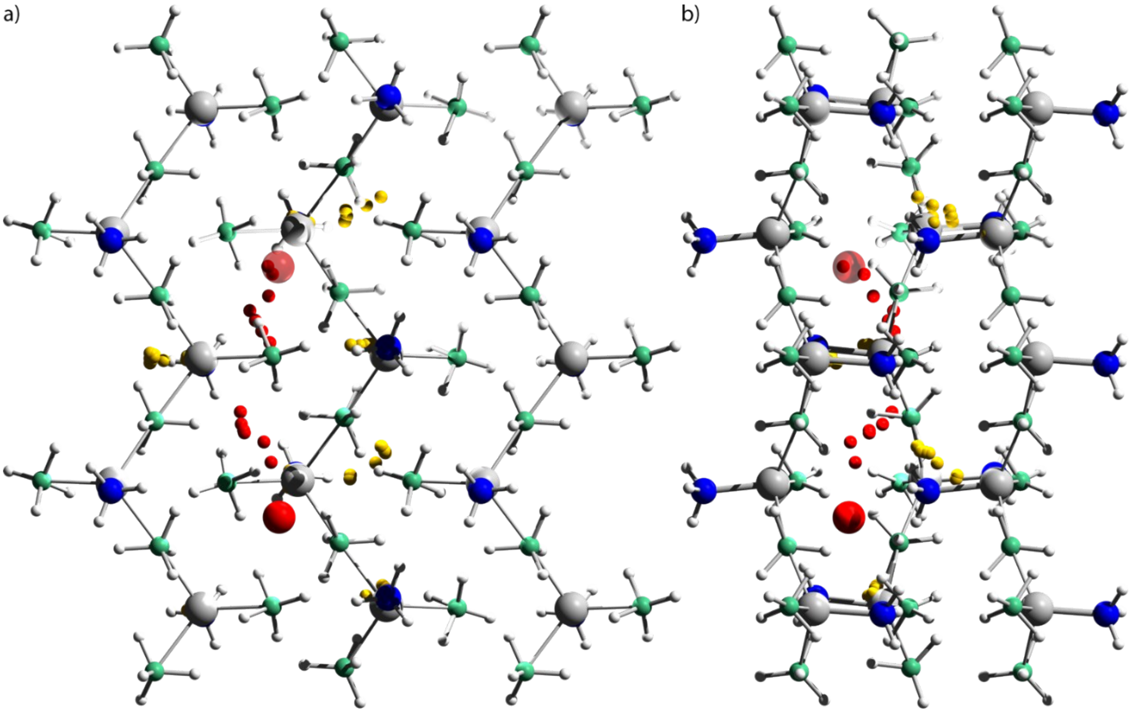

**Figure S9** Migration pathway of interstitial $Mg^{2+}$ (red) in $Mg(BH_4)_2 \cdot NH_3$, which is associated with significant displacement of lattice $Mg^{2+}$ (yellow). a) Top view on $\vec{a}$-$\vec{b}$ plane and b) top view on $\vec{c}$-$\vec{b}$ plane. Red dots correspond to interstitial $Mg^{2+}$ positions of snapshots **a** to **n** from Fig. S8. Yellow dots show displacement of lattice magnesium during migration. Only displaced positions of Mg are shown, all other atoms are fixed on their lattice positions. In red (bigger diameter) the position of the initial position of the Mg interstitial is shown. Translated by one lattice vector a second more transparent interstitial as final state of the migration pathway is shown.

**Table S2.** Maximal displacement of lattice magnesium ions and coordination number of the interstitial for different snapshots of the ion migration pathway shown in Fig. S8a.

| **Structure according to snapshots** | **Maximal displacement of lattice $Mg^{2+}$ [Å]** | **CN d(M-X) < 2.6 Å** | **Long range CN d(M-X) < 3.0 Å** |
|---|---|---|---|
| **a** | 2.58 | 7 | 8 |
| **b** | 2.58 | 7 | 8 |
| **b'** | 2.56 | 7 | 8 |
| **c** | 2.65 | 7 | 8 |
| **c'** | 2.66 | 6 | 9 |
| **d** | 2.68 | 8 | 8 |
| **d'** | 2.44 | 8 | 9 |
| **e** | 2.13 | 8 | 8 |
| **f** | 2.09 | 7 | 8 |
| **f'** | 1.65 | 7 | 7 |
| **g** | 1.60 | 8 | 9 |
| **h** | 1.55 | 8 | 8 |
| **i** | 1.66 | 7 | 8 |
| **j** | 1.88 | 8 | 8 |
| **j'** | 1.86 | 7 | 9 |
| **k** | 1.88 | 6 | 8 |
| **l** | 1.94 | 7 | 8 |
| **l'** | 1.88 | 7 | 8 |
| **m** | 2.13 | 8 | 9 |
| **n** | 2.56 | 7 | 8 |

## Characterisation of $MgCl_2\cdot 2NH_3$

$MgCl_2\cdot 6NH_3$ was synthesised by reaction of anhydrous $MgCl_2$ (purity, 99.9 w%; Sigma-Aldrich) with dry ammonia gas at a pressure of 1 bar for 2 hours at room temperature. The as-synthesised $MgCl_2\cdot 6NH_3$ was heated to 100 °C for three hours under dynamic vacuum to obtain $MgCl_2\cdot 2NH_3$. PXD pattern in Fig. S10 shows the synthesis results in pure $MgCl_2\cdot 2NH_3$. However, the Nyquist plots of the as-synthesised $MgCl_2\cdot 2NH_3$ in Fig. S11 do not show a typical semi-circle but only some scattered points, indicating very low ionic and electronic conductivity of $MgCl_2\cdot 2NH_3$, $\sigma < 10^{-10}$ S cm$^{-1}$ according to the sensitivity of our impedance instrument. Thus, we conclude that $MgCl_2\cdot 2NH_3$ is an insulating material at moderate temperatures.

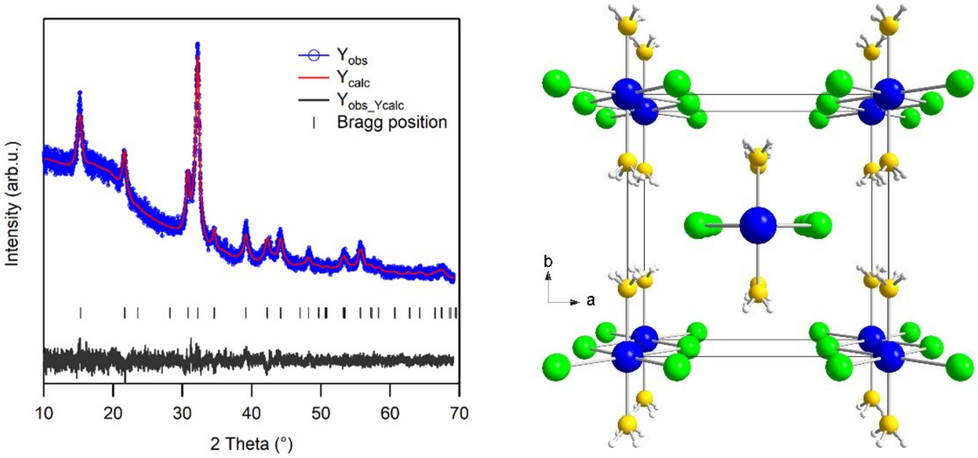

**Figure S10. Left:** Rietveld refinement plot of PXD data measured at room temperature, $\lambda$ = 1.54056 Å, for $MgCl_2\cdot 2NH_3$, showing experimental (blue circles) and calculated (red line) PXD patterns, and a difference plot below (black line). $MgCl_2\cdot 2NH_3$: space group *Cmmm*, unit cell parameters $a$ = 8.1810(2), $b$ = 8.2067(2), $c$ = 3.7550(1) Å. Tick ($MgCl_2\cdot 2NH_3$, ICSD_202459, 100%). Final discrepancy factors: $R_p$ = 4.24 %, $R_{wp}$ = 5.56 % (not corrected for background), $R_p$ = 16.8 %, $R_{wp}$ = 15.2 % (conventional Rietveld R-factors), $R_{Bragg}(MgCl_2\cdot 2NH_3)$ = 2.02 %, and global $\chi^2$ = 3.61. **Right:** Crystal structure of $MgCl_2\cdot 2NH_3$. Mg, Cl, N and H are in blue, green, yellow and grey, respectively.

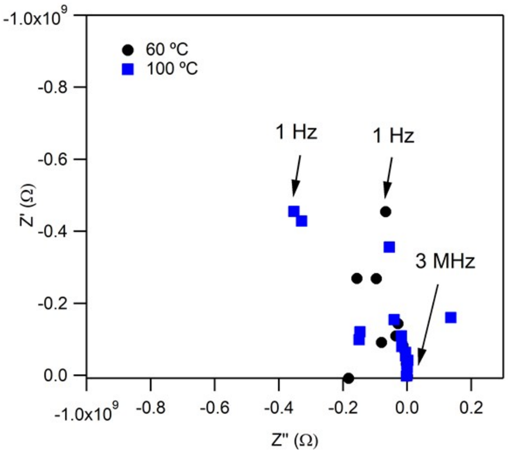

**Figure S11.** Nyquist plots of $MgCl_2 \cdot 2NH_3$ at 60 and 100 °C.

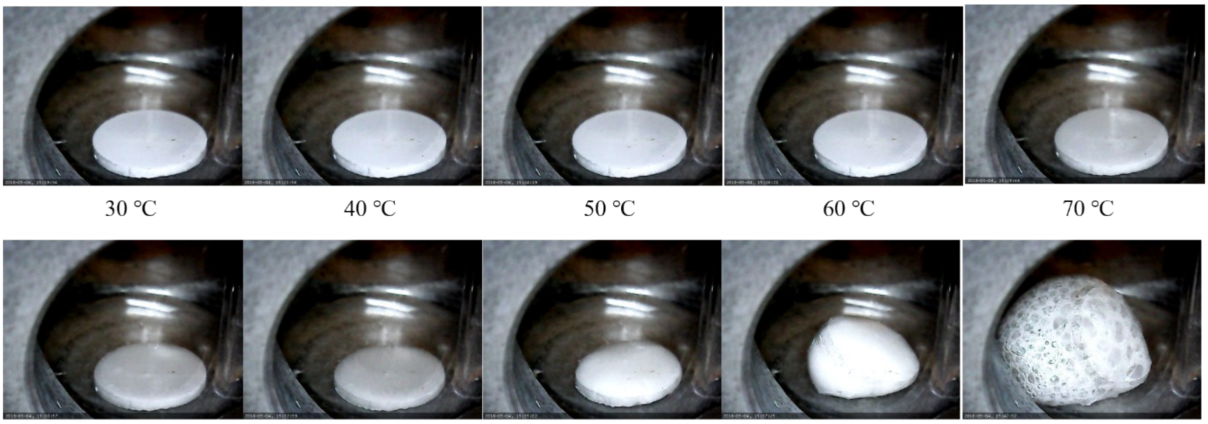

30 °C 40 °C 50 °C 60 °C 70 °C

80 °C 90 °C 100 °C 110 °C 136 °C

**Figure S12.** Photographic thermal analysis images of $Mg(BH_4)_2 \cdot NH_3$

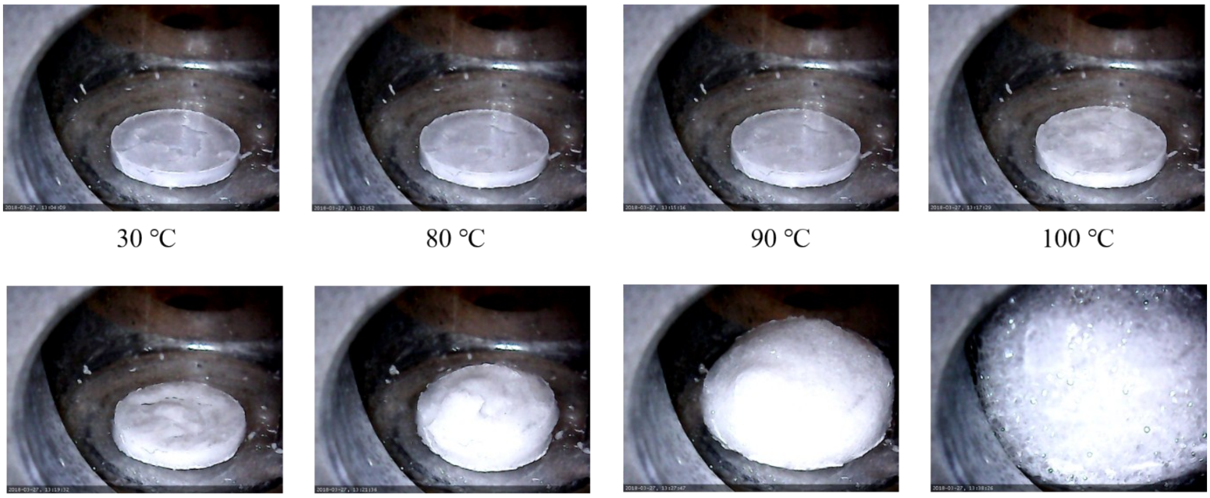

30 °C 80 °C 90 °C 100 °C

110 °C 120 °C 150 °C 200 °C

**Figure S13.** Photographic thermal analysis images of $Mg(BH_4)_2 \cdot 2NH_3$

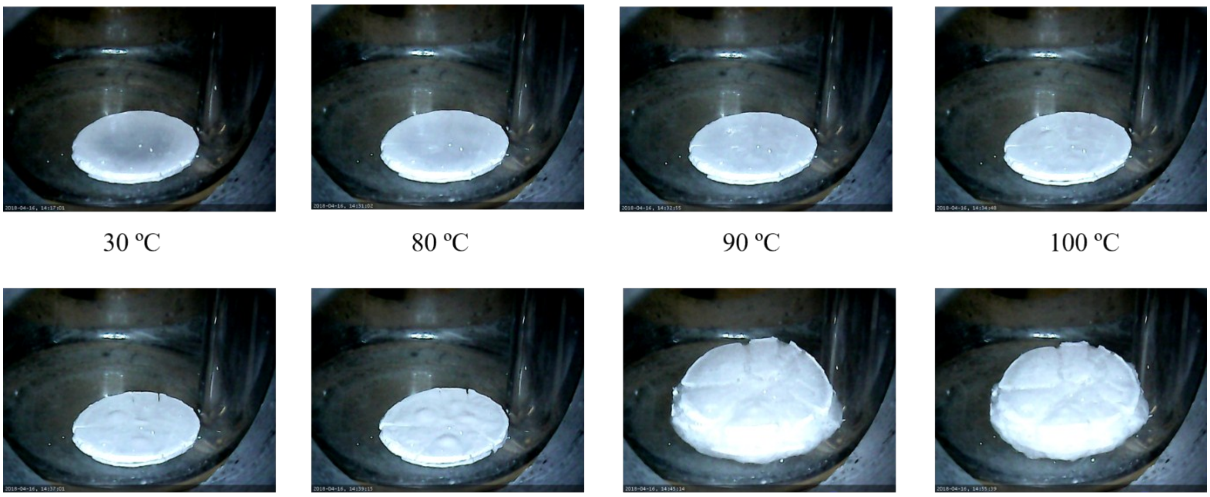

30 °C 80 °C 90 °C 100 °C

110 °C 120 °C 150 °C 200 °C

**Figure S14.** Photographic thermal analysis images of $Mg(BH_4)_2 \cdot 3NH_3$

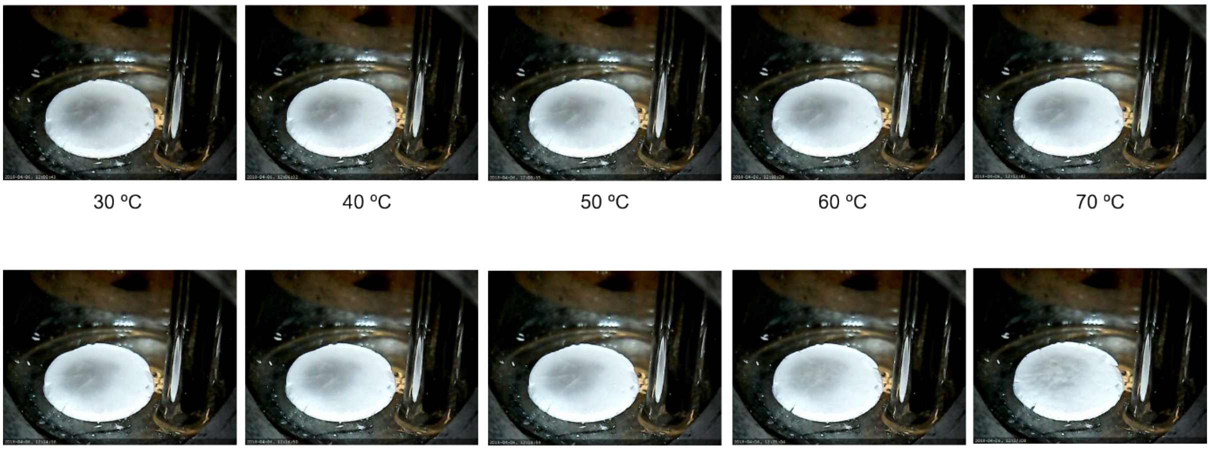

30 °C 40 °C 50 °C 60 °C 70 °C

80 °C 90 °C 100 °C 110 °C 120 °C

**Figure S15.** Photographic thermal analysis images of $Mg(BH_4)_2 \cdot 6NH_3$

### Qualitative comparison of Mg-migration pathways in $Mg(BH_4)_2{\cdot}xNH_3$ (x = 1, 2, 3, 6)

A qualitative analysis of the mechanisms of Mg-ion migration in the ammoniated $Mg(BH_4)_2$ compounds suggests a reliance on flexible ligands. Fig. S16 shows a proposed, simplified ion-migration mechanism in $Mg(BH_4)_2{\cdot}NH_3$ for comparison between the different ammoniates, x = 1, 2, 3 or 6. The blue tetrahedra show the framework Mg ions as they are positioned in the static structure, while the orange and green tetrahedra show available, distorted tetrahedral positions. Following the movement of the Mg, starting from the blue tetrahedron in the top left corner, Mg can move through the edge of the tetrahedron to the orange tetrahedron. Both the ammonia and one of the borohydrides (marked with an asterisk) are only coordinated to the migrating Mg, hence they are expected to relatively easily rearrange to form a regular tetrahedron. Considering the crystal structure as a whole, no symmetry is broken by moving the $BH_4$ and $NH_3$ groups in the B-plane (spanned by the *a* and *c* axes) as they are both positioned in the 4c Wyckoff site (x, 0.25, z). From the orange tetrahedron, the migrating Mg can move through the tetrahedron face to the green tetrahedron, and form a bond to the $NH_3$ below, while breaking the bond to the previous $NH_3$, and finally move to a position which is symmetry equivalent to the original position, through the face of the green tetrahedron.

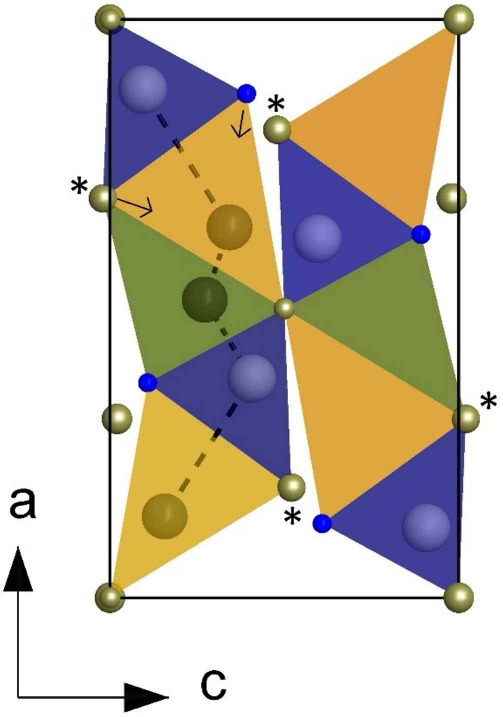

**Figure S16.** Qualitative ion-migration pathway in $Mg(BH_4)_2{\cdot}NH_3$ showing lattice sites (blue tetrahedra) and distorted interstitial sites (green and orange tetrahedra). Asterisks specify terminal $BH_4^-$-groups. The atoms are color-coded: green: boron, blue: nitrogen: white: lattice magnesium, dark grey: interstitial magnesium.

In the case of $Mg(BH_4)_2{\cdot}2NH_3$, the additional ammonia results in isolated $[Mg(NH_3)_2(BH_4)_2]$ tetrahedra with no bridging $BH_4^-$ groups, thus potentially increasing the flexibility of the structure even further as compared to $Mg(BH_4)_2{\cdot}NH_3$. However, the geometry of the crystal structure suggests that a significant, but gradual rearrangement of the structure is necessary to form viable interstitial sites for the migrating Mg-ion. A visual representation is challenging since each consecutive site of the $Mg^{2+}$ migration is more distorted and polyhedral corners formed by ammonia may be missing.

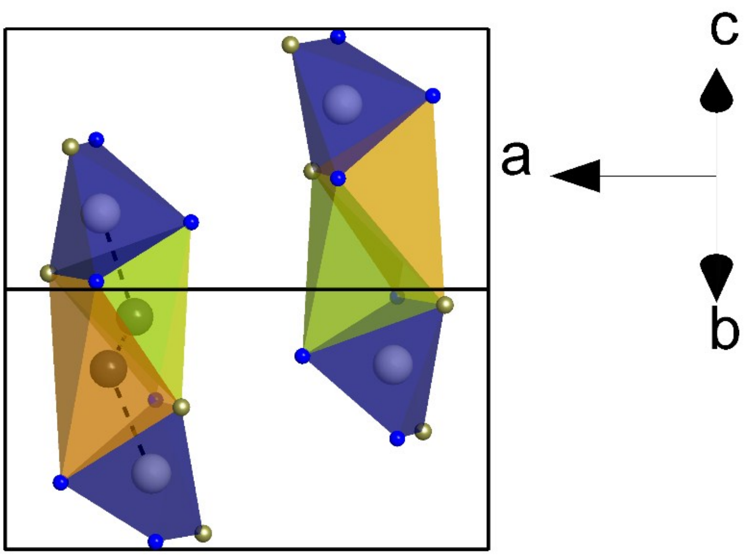

**Figure S17.** Qualitative ion-migration pathway in $Mg(BH_4)_2{\cdot}3NH_3$ showing lattice sites (blue tetrahedra) and distorted interstitial sites (green and orange tetrahedra). The atoms are color-coded: green: boron, blue: nitrogen: white: lattice magnesium, dark grey: interstitial magnesium.

The structure of $Mg(BH_4)_2{\cdot}3NH_3$ consists of isolated $[Mg(NH_3)_3(BH_4)_2]$ molecular units in a distorted bipyramidal geometry (Fig. S17). The polyhedra are connected through their faces, however, the interstitial polyhedra appear to be more distorted as compared to the interstitial sites in $Mg(BH_4)_2{\cdot}NH_3$.

Compared to $Mg(BH_4)_2{\cdot}xNH_3$ ($x$ = 1, 2), there are no intermediate sites where all original ammonia groups remain bound to the migrating Mg-ion cation after a jump (yellow tetrahedra Fig. S17). This likely limits the mobility of $Mg^{2+}$, as ammonia has to reposition and bind to another $Mg^{2+}$ as part of the jump of the migrating Mg-ion.

Furthermore, due to the crystallographic site restrictions of the borohydride groups situated in the 4c site (x, 0.25, z) symmetry may be lowered to form a more ideal tetrahedral coordination. The more complex structure and resultingly more complex dynamics of the cation jumps are likely the reason for the significantly lower ionic conductivity compared with $Mg(BH_4)_2{\cdot}xNH_3$ ($x = 1, 2$).

In the case of $Mg(BH_4)_2{\cdot}6NH_3$ there are no obvious interstitial sites for Mg migration without a significant rearrangement of the structure.

## References

1. R. H. Crabtree, P. E. M. Siegbahn, O. Eisenstein, A. L. Rheingold and T. F. Koetzle, *Acc. Chem. Res.,* 1996, **29**, 348-354.
2. T. Richardson, S. de Gala, R. H. Crabtree and P. E. M. Siegbahn, *J. Am. Chem. Soc.* 1995, **117**, 12875-12876.
3. Y. Yang, Y. Liu, Y. Li, M. Gao and H. Pan, *Chem. Asian J.,* 2013, **8**, 476-481.
4. Y. Yang, Y. Liu, Y. Li, M. Gao and H. Pan, *J. Phys. Chem. C*, 2013, **117**, 16326-16335.